Selective Stimulation of Sensory Fascicles in the Ulnar Nerve for Amputees

By: Amith Chitneni & Owen Anderson

Objective and Hypothesis

Using extraneural cuff, interfascicular, and intrafascicular electrode placements, the project's goal is to evaluate the selectivity and efficiency of peripheral sensory nerve stimulation with monopolar, bipolar, or tripolar configurations, and either extraneural, interfascicular, or intrafascicular electrode placements. Using COMSOL, an ulnar nerve model is used to compute voltage distributions for each of the nine conditions, and these results were analyzed in NEURON using the McIntyre-McNeal-Grill model to simulate peripheral nerve stimulation. We hypothesize that the tripolar intrafascicular stimulation will yield the highest selectivity: the tripolar electrode placement will have two return electrodes that confine the current from neighboring fascicles, and the intrafascicular setup will have the electrode placed directly inside the fascicle to lower the amplitude required for an AP threshold (Becker et al., 2023). The goal is to inform future approaches that aim to selectively stimulate the sensory fascicle in the ulnar nerve for applications to functional electrical stimulation and sensory prostheses.

Methods: COMSOL Model

Our model began with a 2D base of the cross-sectioned ulnar nerve with four fascicles. The "difference" Boolean operator was used to segment the circles and ellipses representing the epineurium layer, the four perineurium layers, and the four endoneurium layers (**Figure 1)**. The extrude function was later used to add a 3D representation of this base, serving as the nerve before the branch, which will be the target for stimulation. The nerve branching was then constructed using the same 2D-to-3D extrude technique and the "difference" operator for proper sectioning/boundaries. The nerve cuff — for the extraneural case — was then built using ellipses and the extrude function. Finally, the saline bath was a 3D ellipsoid that covered the entirety of the nerve and served as the electrically grounded domain (**Figure 2**).

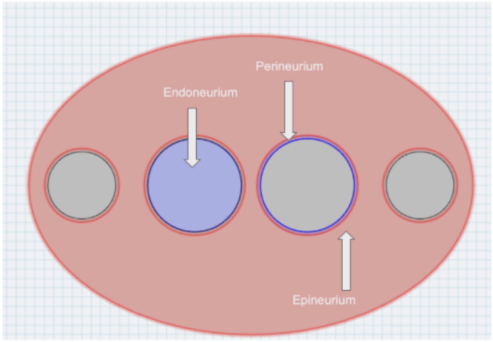

Figure 1: The 3 different segmented layers within the base of the

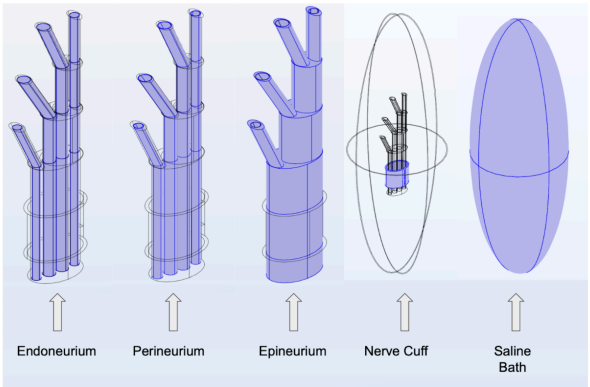

Figure 2: The 3d representation of the 3 segmented layers, the cuff, and the saline bath.

From there, the electrodes themselves were created. They were modelled as small 3D patches

and placed in their appropriate locations for the 9 different test conditions. In our model, the 3rd fascicle was treated as the primary sensory fascicle,e and therefore the electrodes were all lined up on this specific fascicle so there can be an even comparison between the conditions. **Figure 3** shows the tripolar configuration for each of the 3 different positions. For the given configurations, the monopole has one anode at +1 mA; the dipole has one cathode at -1 mA and one anode at +1 mA; the tripolar has one cathode at -1 mA and two anodes at +0.5 mA each.

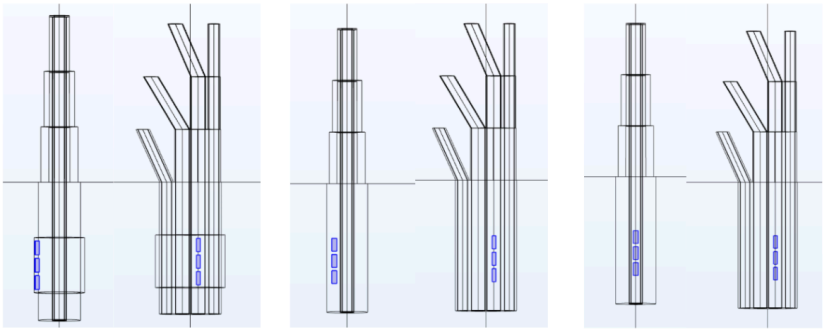

Figure 3: The electrode positions for the 3 different placements. The tripolar electrode configurations is shown.

Once all proper segmentation and graphics were completed, the material conductivities and permeabilities were assigned. The endoneurium exhibited both transverse and longitudinal conductivities of 0.571 S/m and 0.0826 S/m, respectively. Thus, the endoneurium was anisotropic with less resistance to current flow horizontally than vertically. The perineurium had an isotropic 0.021 S/m electrical conductivity, serving as a resistive layer, and the epineurium had an isotropic conductivity of 0.0826 S/m. Additionally, the nerve cuff was modelled as silicone with a conductivity of 1 × 10^-11 S/m, and the electrode patch was composed of gold with a conductivity of 4.1 × 10^7 S/m. These values can all be seen in **Table 1 (**Kinouchi et al. 1997). Regarding assumptions, the model assumes uniform tissue properties within each layer, no temperature rise, no electrochemical reactions, and perfect-conductor electrodes. A free tetrahedral mesh was used to discretize the electrode-tissue interface, and a boundary-layer mesh was also placed within the perineurial entities. Additionally, the PARDISO direct solver was used with a zero initial potential and standard tolerances under stationary conditions.

Table 1: The conductivities of the various regions within the nerve

Model Regions	Conductivity σ (S/m)
Endoneurium Transverse	0.571
Endoneurium Longitudinal	0.0826
Perineurium	0.021
Epineurium	0.0826
Silicone Cuff	1 × 10^-11
Electrode Patch	4.1 × 10^7

Lastly, the “solve” button was utilized to calculate the voltages over space. From there, a 3D “cut-line” was inserted into each of 4 fascicles, which spatially sampled a voltage vs. arc length position trace. These four traces for each of 9 the test conditions could then be fed into NEURON.

Methods: NEURON Model

We simulated peripheral nerve activation in NEURON using the McIntyre–Richardson–Grill (MRG) myelinated axon model. The model consists of 21 nodes of Ranvier connected by paranodal (MYSA/FLUT) and internodal (STIN) segments, with diameter-specific electrical properties tuned for mammalian myelinated fibers at 37 °C (McIntyre et al., 2002). Each segment includes an extracellular mechanism, allowing externally applied fields to be imposed directly. In COMSOL, as aforementioned, voltage profiles were obtained using "cut-lines" that characterize the voltage distribution along each fascicle. We interpolated each fascicle's COMSOL arc-length profile onto every segment center of the MRG axon, using a linear scale map by default. The spatially mapped, unit-voltage profile is multiplied by a rectangular pulse (delay 1 ms, width 0.2 ms, and scaled by amplitude) to form per-segment extracellular time-series in mV (**Fig. 4**). That scale is multiplied by the unit spatial profile to form per-segment extracellular voltages. We then called NEURON's Vector.play() function, which attaches each segment's time series to its extracellular potential. Finally, we ran the simulation using a timestep of 0.025 ms for 5 ms. We recorded transmembrane voltage (Vm) at the central node to quantify activation.

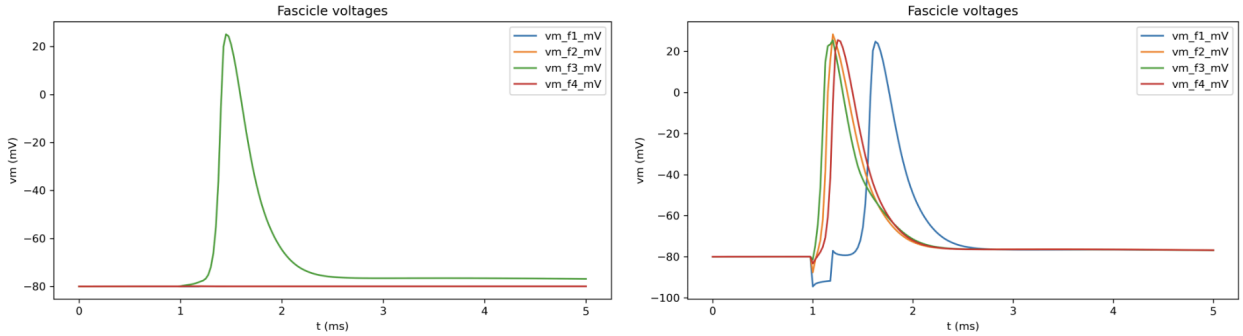

Figure 4: A) Example voltage trace showing fascicle 3 firing under 0.03A current using the bipolar, intrafascicular configuration and position. B) Example voltage trace showing all fascicles firing under 1.0A current using monopolar, interfascicular placement and electrode configuration.

Methods: Selectivity Analysis

Amplitude sweeps — which are time-series obtained by titrating amplitudes from 5e-05 to 2 times the input current of 1 mA — were applied to each electrode configuration/position to obtain the threshold for fascicle activation. For each sweep, the peak Vm for each fascicle was determined at every amplitude scale (**Fig. 5**), and normalized by dividing by that fascicle's own maximum over all amplitudes in the sweep to get a normalized maximum voltage V_i for each fascicle (**Eq. 1**). We chose to use the Selectivity at each amplitude was then computed from the normalized voltage values (**Eq. 2, Fig. 6**) (Yoo et al. 2004). Finally, selectivity was averaged across the sweep for each fascicle in each configuration, enabling direct comparison (e.g., fascicle 3) across all conditions.

$$V_{i,norm} = \frac{V_i}{max} \quad (1)$$

$$S_i = \frac{V_{i,norm}}{\sum_j V_{j,norm}} \quad (2)$$

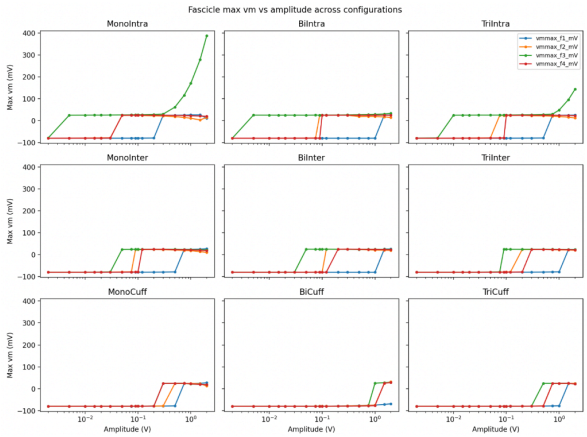

Figure 5: Average selectivity across a current sweep for each fascicle across each combination of electrode configuration and position.

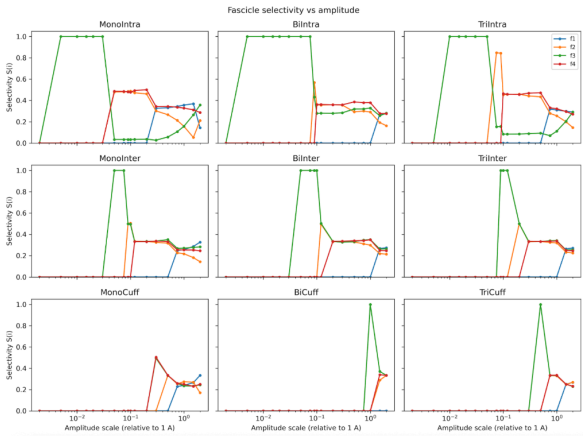

Figure 6: Selectivity for each fascicle across the voltage sweep.

Statistical Analysis:

To determine which stimulation configuration has the highest average selectivity for fascicle three across the current sweeps, we employed an approximate mixed-effects approach. We used an ordinary least squares model with categorical fixed effects for configuration and amplitude. We estimated marginal means per configuration averaged over the observed amplitude distribution, and used pairwise configuration contrasts with Holm-adjusted p-values. This allowed us to assess the statistical significance ($p < 0.05$) of differences between stimulation configurations/electrode placements for each fascicle.

Results:

For fascicle 3 — the sensory fascicle — the bipolar intrafascicular configuration was the most favorable (0.419 ± 0.060). The bipolar intrafascicular configuration beats the bipolar cuff, the monopolar cuff, and the tripolar cuff. The estimated marginal means (mean selectivity $\pm$ standard error across the current sweep) favored the monopolar intrafascicular configuration/placement for fascicle 1 (0.078 ± 0.012), and the monopolar intrafascicular configuration significantly exceeded bipolar cuff, bipolar interfascicular, bipolar intrafascicular, tripolar cuff, and tripolar interfascicular. For fascicle 2, the tripolar intrafascicular configuration was favored (0.201 ± 0.026). The tripolar intrafascicular configuration beats the bipolar cuff, the tripolar cuff, and the monopolar cuff configurations, while the monopolar intrafascicular beats the bipolar cuff and the tripolar cuff. For fascicle 4, the monopolar intrafascicular configuration was the best, beating the bipolar cuff, the bipolar intrafascicular, the monopolar cuff, the

monopolar interfascicular, the tripolar cuff, and the tripolar interfascicular. Additionally, the tripolar intrafascicular and bipolar intrafascicular configurations beat the bipolar cuff (Fig. 7,8).

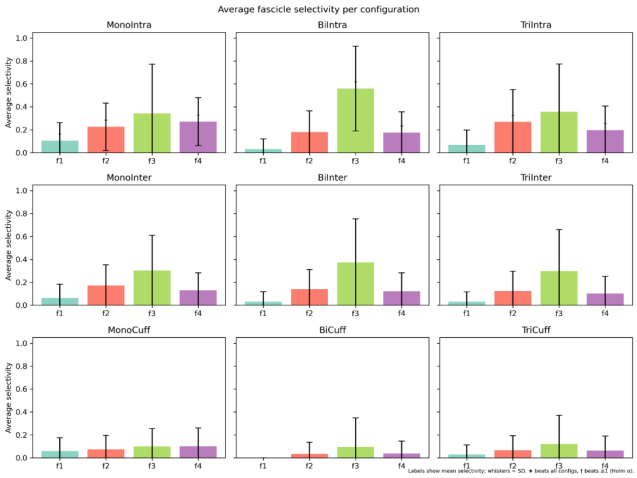

Figure 7: Average selectivity across a current sweep for each fascicle across each combination of electrode configuration and position.

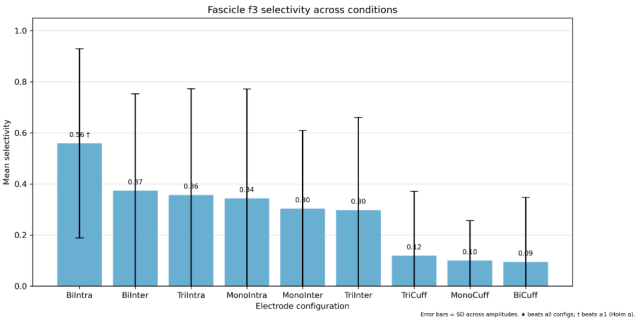

Figure 8: Average selectivity for fascicle 3 across a current sweep for each combination of electrode configuration and position

Conclusion and Discussion:

In this study, we evaluated how electrode placement (extraneural, interfascicular, and intrafascicular) and configuration (monopolar, bipolar, and tripolar) influence selectivity during sensory fascicle stimulation. By using a COMSOL 3D model of the ulnar nerve and the MRG myelinated axon model in NEURON, we could directly compare all 9 possibilities.

Across electrode placement conditions, the intrafascicular case consistently showed the highest selectivity, highlighting the importance of minimizing the electrode-axon distance and confining current spread to prevent neighboring fascicles from being stimulated. Among these cases, the intrafascicular bipolar stimulation was the most selective configuration for fascicle 3 — the target sensory fascicle for sensory restoration in amputees — as it had the highest mean selectivity across the amplitude sweep. This finding showed that the bipolar intrafascicular conditions had an effective balance between spatial focusing of the electric field and efficient depolarization of targeted axons.

Theoretically, while a tripolar configuration should offer the best current confinement, as our hypothesis stated, its performance in our study was largely inconsistent with our original hypothesis. This electrode configuration required higher effective amplitudes, which suggested over-constraint of the field within small intrafascicular volumes. Additionally, the monopolar configuration cases experienced poorer selectivity due to broader current spread, as theory suggests. Despite differences between theoretical/experimental results and limitations in our assumptions, integrating COMSOL-derived potentials with NEURON-based activation analysis provided a robust framework for quantitatively comparing stimulation strategies.

Overall, while we did not find that a single configuration/position combination statistically beat out all other combinations, this study provides strong computational evidence that bipolar intrafascicular stimulation is promising for the most selective stimulation of a fascicle for sensory restoration, particularly for upper-limb neuroprosthetic applications such as those involving the ulnar nerve. Future work will improve biophysical realism, incorporate efficiency metrics alongside selectivity, and add additional geometries/pulse parameters to the analysis. Cumulatively, such efforts can guide the next-generation peripheral nerve stimulation that minimizes off-target activation and power requirements, while maximizing functional specificity.

References:

1: Becker, Rachel E. and Biagio Manna . “Anatomy, Shoulder and Upper Limb, Ulnar Nerve.” *StatPearls*, StatPearls Publishing, 24 July 2023.
2: Kinouchi, Y et al. “Fast in vivo measurements of local tissue impedances using needle electrodes.” *Medical & biological engineering & computing* vol. 35,5 (1997): 486-92. doi:10.1007/BF02525528
3: McIntyre, Cameron C et al. “Modeling the excitability of mammalian nerve fibers: influence of afterpotentials on the recovery cycle.” *Journal of neurophysiology vol*. 87,2 (2002): 995-1006. doi:10.1152/jn.00353.2001
4: Yoo, Paul B et al. “Selective stimulation of the canine hypoglossal nerve using a multi-contact cuff electrode.” *Annals of biomedical engineering* vol. 32,4 (2004): 511-9. doi:10.1023/b:abme.0000019170.74375.fb